Superlattices and Microstructures 79 (2015) 29–37

Contents lists available at ScienceDirect

Superlattices and Microstructures

journal homepage: www.elsevier.com/locate/superlattices

On the origin of white photoluminescence from ZnO nanocones/porous silicon heterostructures at room temperature

Oscar Marin [a,*], Gustavo Grinblat [a], Ana María Gennaro [b,d], Mónica Tirado [c], Roberto R. Koropecki [b], David Comedi [a]

[a] CONICET, LAFISO y Nanoproject, Facultad de Ciencias Exactas y Tecnología, Universidad Nacional de Tucumán, Avenida Independencia 1800, 4000 San Miguel de Tucumán, Argentina
[b] Instituto de Física del Litoral, CONICET-Universidad Nacional del Litoral, Güemes 3450, 3000 Santa Fe, Argentina
[c] CONICET, LNPD y Nanoproject, Facultad de Ciencias Exactas y Tecnología, Universidad Nacional de Tucumán, Avenida Independencia 1800, 4000 San Miguel de Tucumán, Argentina
[d] Departamento de Física, Facultad de Bioquímica y Ciencias Biológicas, Universidad Nacional del Litoral, Ciudad Universitaria, 3000 Santa Fe, Argentina

ARTICLE INFO

Article history:
Received 17 October 2014
Accepted 15 December 2014
Available online 20 December 2014

Keywords:
ZnO nanocones
Photoluminescence
Electron paramagnetic resonance
White emission
Porous silicon

ABSTRACT

ZnO nanocones were grown on porous silicon (PS) by vapor transport at different temperatures and O_2 flow rates without metal nanocatalysts. The ZnO/PS heterostructures were studied by electron microscopy, and by photoluminescence and electron resonance (EPR) spectroscopies. Samples emitted strong white PL, opening potential application for white light illumination. The photoluminescence spectra were found to include five main components centered at 1.84, 2.06, 2.30, 2.48 and 3.31 eV. The components at 2.48 and 2.06 eV were related to oxygen vacancies in ZnO, that at 2.3 eV to Zn vacancies and the one at 1.84 eV to the PS substrate. The low excitonic emission intensity at 3.31 eV and the observed rough ZnO nanocone morphology suggest the presence of surface trap states. EPR shows a $g \sim 2.006$ line attributed to Zn divacancies. The absence of the $g = 1.96$ line, attributed to conduction band electrons, suggests strong carrier depletion.

* Corresponding author. Tel.: +54 381 4364093; fax: +54 381 436 4157.
E-mail addresses: omarin@herrera.unt.edu.ar, alquimarin@gmail.com (O. Marin).

http://dx.doi.org/10.1016/j.spmi.2014.12.016
0749-6036/

1. Introduction

Porous silicon (PS) and ZnO are widely studied semiconducting materials due to their potential applications in optoelectronics [1,2], biotechnology [3,4], solar cells [5,6], sensing [7,8], and others. The great interest on these materials is partly due to their low production cost and interesting chemical and physical properties. Specifically, ZnO is a wide direct band gap (3.37 eV) with large exciton binding energy (60 meV) [9,10], high chemical stability, and offers the possibility of obtaining a myriad of nanoscale morphologies such as nanowires (NWs), nanocones, hierarchical nanostructures, nanorods and nanoflowers [9,11,12]. There are several techniques for ZnO nanostructure growth, including electrophoretic deposition [13], hydrothermal synthesis [8] and carbothermal reduction with vapor transport (VT) [14], the latter being the most used and studied technique. In particular, to obtain ZnO NWs using the VT technique the use of Au nanoclusters, which act as catalysts and nucleation centers on the growth substrates, is often necessary [14]. In order to avoid the use of gold, several research groups have tried various types of substrates, finding promising results with PS [15–17]. In addition to the possibility of avoiding the use of Au nanoclusters, the deposition of ZnO on PS is an attractive way of integrating the ZnO with the silicon-based electronics technology [18]. For instance, ZnO/PS could be used for the development of bi-luminescent or white light emitting devices. The emission properties of both ZnO and PS have been studied thoroughly and they have been found to strongly depend on the nanostructure morphology. White light emission has been reported for ZnO/PS nanocomposites grown by sol–gel routes [19,20].

In this paper, ZnO/PS structures grown by VT and electrochemical anodization at different fabrication conditions are studied using scanning electron microscopy (SEM), photoluminescence (PL) and electron paramagnetic resonance (EPR) spectroscopies. The conditions for ZnO cone-like NW growth without the need of metallic nanocatalysts are found. The ZnO/PS samples are found to emit white light. The distinct components of the PL and corresponding EPR spectra are identified and their origin elucidated.

2. Experimental method

The PS substrates were prepared by electrochemical anodization of crystalline n-type (phosphorus doped) silicon, with resistivities between 1–10 Ω cm and ⟨100⟩ orientation. The crystalline silicon wafers were anodized in a 1:2 solution of HF (50%):ethanol for 15 min under constant current density (20 mA/cm^2) and illumination (halogen lamp with 300 W of power placed at 14 cm of the sample). The samples were rinsed with ethanol and dried with a N_2 flow. The PS substrates obtained were kept in darkness to avoid photo-oxidation processes.

The ZnO depositions were carried out by carbothermal reaction with VT in a quartz tube placed in a horizontal tubular furnace under constant Ar and O_2 flow rates. An alumina boat with mixed ZnO and C (graphite) powders in 1:1 mass proportion was placed at 1.5 cm from the center of the furnace, while the as-prepared PS substrates (without Au nanoclusters) were placed at 19.5, 21.5 and 23.5 cm from the center of the furnace downstream. The ZnO:C mixture was heated to 1100 °C with a rate of 27 °C/min and then kept at 1100 °C for 20 min. The temperatures reached at the positions where the PS substrates had been placed were 950, 890 and 840 °C, respectively. In order to study the effect of the O_2 flow on the ZnO structure and PL, samples with two different O_2 flow rates were grown (8 and 40 sccm), while the Ar flow rate was kept constant at 125 sccm for all samples.

PL spectra were recorded by illuminating the samples with a He–Cd laser at a wavelength of 325 nm with 15 mW power. The experiments were carried out in a backscattering arrangement. The emitted light was focalized on a CCD spectrometer with two biconvex lenses. A filter was placed before the spectrometer to eliminate scattered laser radiation. The morphology of samples was characterized with SEM. The EPR experiments were carried out on a Bruker EMX-Plus EPR Spectrometer in the X band.

3. Results and discussion

Fig. 1 shows SEM micrographs of PS substrate and ZnO nanostructures grown on PS for different temperatures and O_2 flow rates. As observed, ZnO nanostructures could be grown on PS substrates without the presence of metallic nanocatalysts. The PS samples studied had a mean pore size of 2 μm and a porosity of ~60%. As seen in Fig. 1(a), in the PS samples some adjacent pores collapsed to form channels with irregular orientation. In other regions, individual pores were preserved. This morphology was common for all samples. All samples studied (Fig. 1(b)–(f)) showed ZnO NWs exhibiting cone-like morphology, i.e. the NW cross sectional area decreases along the NW axis from bottom to the top. The growth of ZnO nanocones has been reported previously [9,21–23], but the growth mechanism is still unknown. Various cone-like ZnO NWs grew from certain common preferential

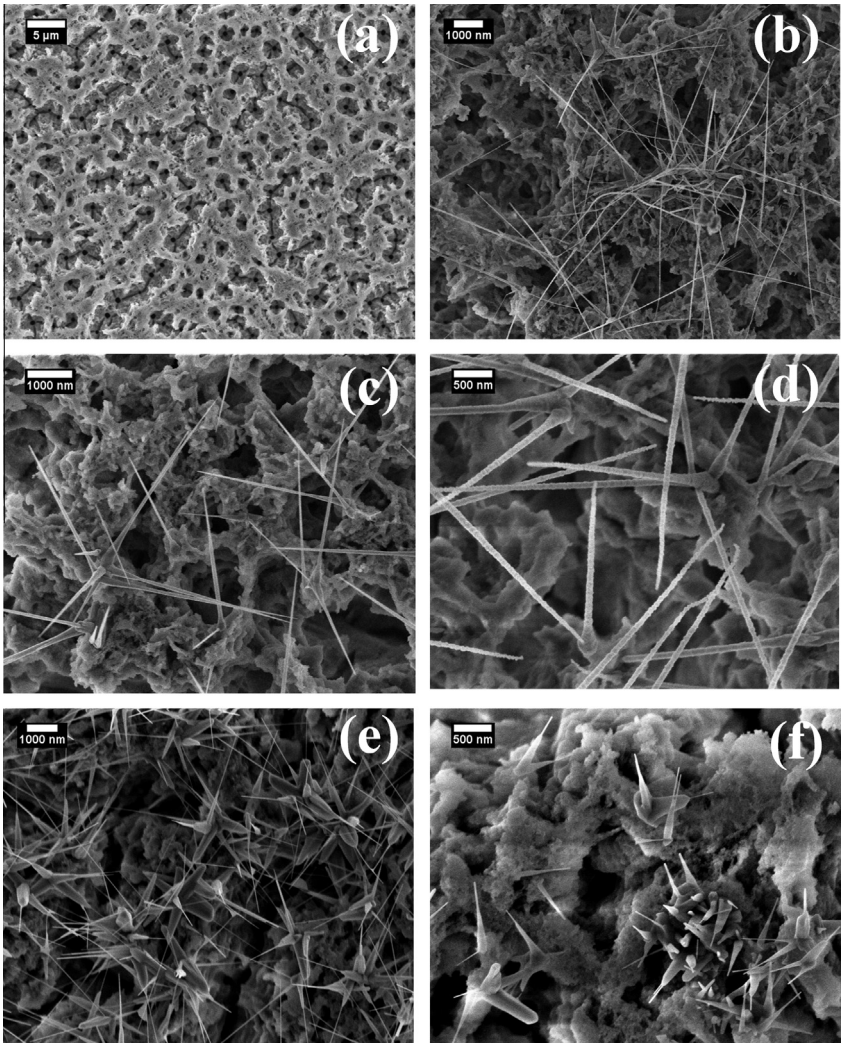

Fig. 1. SEM micrographs of PS and ZnO nanocones grown on PS. (a) PS substrate held at 950 °C with an O_2 flow of 8 sccm. (b)–(d) ZnO nanocones grown at 950, 890 and 840 °C, respectively with an O_2 flow rate of 8 sccm. (e) and (f) ZnO nanocones grown at 950 and 840 °C, respectively with an O_2 flow rate of 40 sccm.

spots at the PS network in different directions. The nanocones surface is rough, indicating faceted growth along the NW walls (most clearly seen in Fig. 1(d)). The ZnO nanocones grown with an O_2 flow rate of 8 sccm (Fig. 1(b)–(d)) showed an average length of about 4 μm with a diameter at the bottom of about 200 nm and at the top of about 10 nm, while for an O_2 flow rate of 40 sccm the average length was 2 μm (Fig. 1(e) and (f)) with diameters similar to those for 8 sccm. The density of ZnO nanocones obtained with an O_2 flow rate of 40 sccm was lower and this is consistent with an incomplete reaction of the ZnO:C mixture observed in this case. The incomplete reaction at large O_2 flow rate could be due to increased oxidation of ZnOx ($x < 1$) species that competes with the intentional carbothermal reduction of the ZnO powder.

Fig. 2 shows the PL intensity of ZnO/PS structures. Typically, ZnO exhibits a PL spectrum with both UV (at about 375 nm) and visible emissions [10,24,25]. The origin of UV emission is related to excitonic recombination, while the visible emission is related to transitions of excited carriers (both electrons and holes) involving lattice defect or surface states [10,25,26].

In our case, the ZnO/PS structures exhibit white light emission with low intensity contribution in the UV (∼375 nm). As observed in Fig. 2, the contribution in the green (∼520 nm) dominates the PL spectra for most of the samples, this dominance being markedly more pronounced for an O_2 flow rate of 40 sccm at the higher temperatures.

The spectral region between 450 and 850 nm was fit in all cases with four Gaussian components, three of which are related to emissions from ZnO and the other from PS. The results of this fitting procedure are shown in Fig. 3 for $T = 890$ °C. It is well known that the red PL in PS is quenched upon UV illumination [27,28]. As can be seen in the insets of Fig 3, the peak at about 680 nm quenches with increasing illumination. Hence, it is reasonable to relate this peak with the PS. As shown in Fig. 3, the components related to ZnO emission are found to be around ∼495, ∼535 and 605 nm, which correspond to 2.48, 2.30 and 2.06 eV, respectively. We note that measurements performed on bare

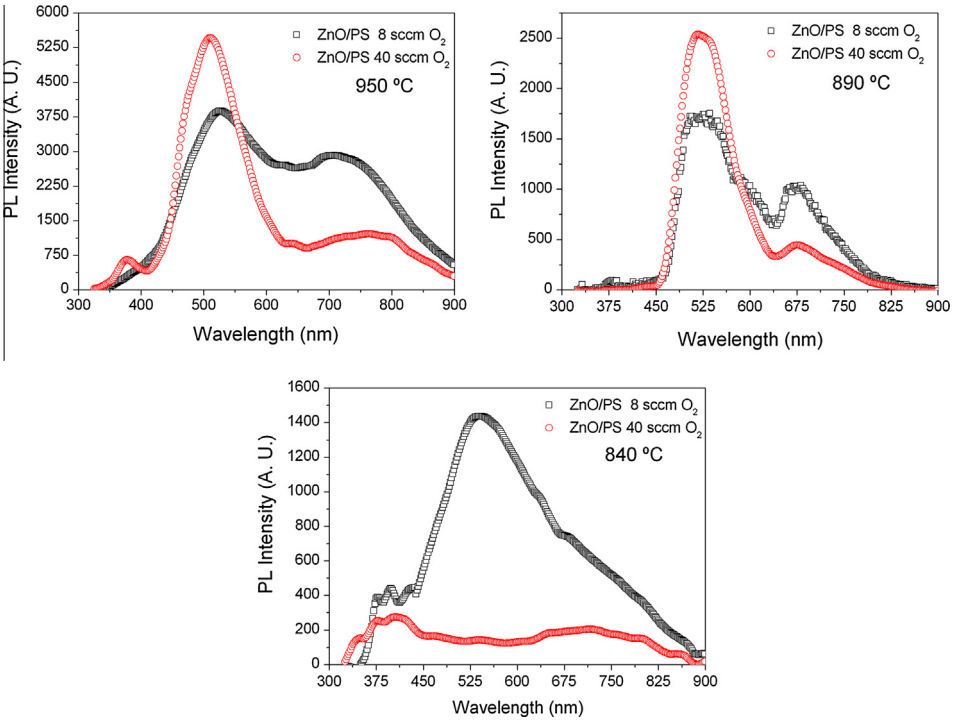

Fig. 2. PL spectra from ZnO nanocones/PS structures.

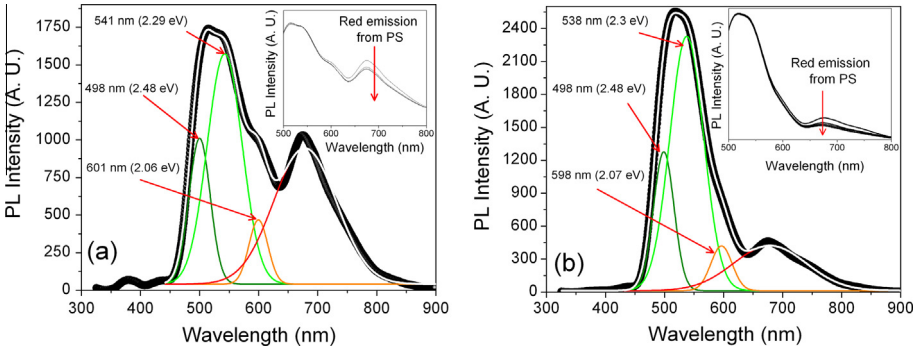

Fig. 3. Multi-Gaussian fitting of PL spectra from ZnO/PS samples for $T = 890$ °C. (a) and (b) Correspond to 8 and 40 sccm of O_2 flow respectively.

PS samples (not shown) showed very little luminescence in the spectral range assigned to ZnO emission, and exhibited typical quenching at ~680 nm induced by laser irradiation. No quenching was found for ZnO luminescence, as expected.

Although it is generally accepted that the visible emission from ZnO is due to defect or surface states, there is considerable controversy on the specific type of defect or surface state that originates each component. The yellow emission (~2.06 eV) has been related to excess oxygen and presence of O_i defects (interstitial oxygen), while the green emission at ~2.48 eV has been related to oxygen deficiency and presence of V_O (oxygen vacancies) [26,29]. However, experimental evidence also suggests that both green and yellow emissions may be due to transitions involving V_O with different charge states [30]. without involving O_i defects.

The simultaneous existence of green and yellow components observed in our samples favors the idea of a common origin for both. If the yellow component was due to oxygen excess, then a higher O_2 flow (40 sccm) should yield a larger O_i concentration and higher yellow emission; so that the ratio ($I_{2.48eV/2.06eV}$) would be lower than for a lower O_2 flow rate (8 sccm). However, the experimental results do not show this general tendency, as shown in Fig. 4.

Hence, we can expect that these emission peaks have a common origin. According to Liao et al. and Zhu et al. [30,31] both the green emission at ~2.48 eV and the yellow emission (~2.06 eV) can originate from electronic transitions related to V_O in ZnO. Specifically, the yellow emission can be attributed to the transitions between electrons in the bottom of the conduction band to doubly ionized

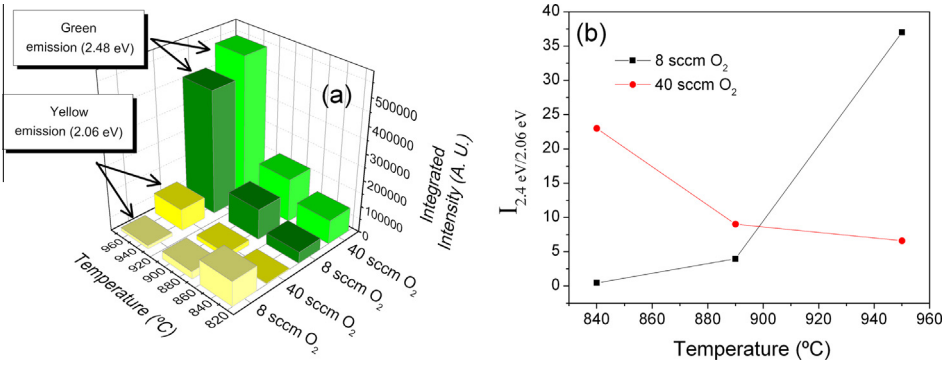

Fig. 4. (a) Integrated intensity of green (2.48 eV) and yellow (2.06 eV) emissions for different growth conditions. (b) Ratio $I_{2.48eV/2.06eV}$ as a function of temperature. (For interpretation of the references to color in this figure legend, the reader is referred to the web version of this article.)

V_O (Vo^{++}), while the green emission at ~2.48 eV can be attributed to transitions between electrons from singly ionized V_O (Vo^{+}) to the valence band [30–32].On the other side, the green emission at ~2.3 eV has been associated with Zn vacancies (V_{Zn}) [33]. Taking into account that V_{Zn} concentration in an oxygen rich atmosphere increases with the O_2 pressure ($V_{Zn} \alpha P_{O_2}^{1/2}$) [34], it is indeed reasonable to relate the peak at ~2.3 eV to V_{Zn} since, as noted in Fig 4(a), this emission is greater for samples grown with 40 sccm of O_2.

At this point, we do not know whether the defect states giving rise to the visible PL are located at the core or at the surface of the ZnO nanostructures, or both. A large concentration of surface states could be expected in the samples studied in this work given the rough morphology of the nanocones surface (Fig. 1). This could explain the low intensity of UV emission from these samples, as the anticorrelation between the UV emission and the surface states concentration has been invoked several times in the literature [34–36]. Furthermore, recent studies of ZnO nanostructures grown on crystalline Si using the same fabrication system and similar growth conditions as the ones used here, have confirmed a correlation between the green emission at ~2.3 eV and surface states [12,37].

We now turn our attention to the EPR measurements in our ZnO/PS samples. The room temperature EPR spectra applying the magnetic field parallel to the ⟨100⟩ PS direction and their respective simulations are shown in Fig. 5(c) and (d). The EPR spectra from PS substrates treated with the same conditions (temperature and Ar/O_2 flow) as those used for the ZnO growth are shown as a reference Fig. 5(a) and (b). First, we note that the signal at $g = 1.96$, typically observed in ZnO in many morphologies [24,38–40], is absent from our spectra (it was not observed for any of the samples studied). The $g = 1.96$ resonance has been attributed to O vacancies [24,38–40], and hence associated with strong luminescence in the visible from ZnO [40,41]. However, alternative interpretations have been also proposed, such as defects related to Zn vacancies or free electrons in the conduction band

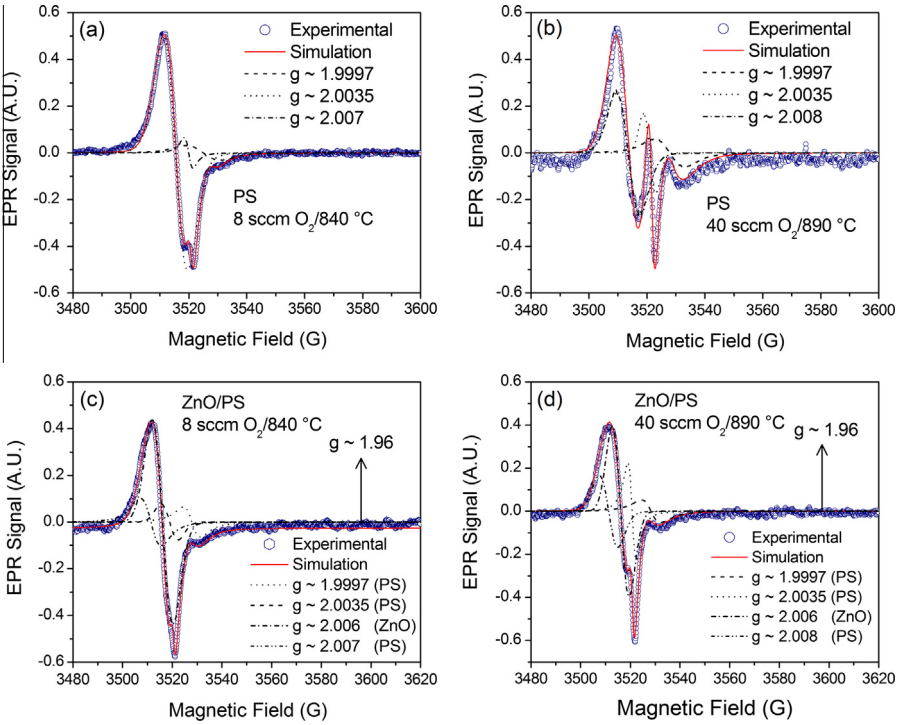

Fig. 5. EPR spectra of PS substrates (a) and (b) and the ZnO/PS heterostructures (c) and (d) for 8 sccm of O_2 at 840 °C and 40 sccm of O_2 at 890 °C. The solid and dotted lines represents the EPR simulations.

[39,42,43]. In our case, the PL data do show strong visible luminescence which we attribute to O and Zn vacancies, but the $g = 1.96$ resonance is absent from our EPR spectra. Hence, our data suggest that the $g = 1.96$ resonance originates from free electrons in the conduction band and not from V_{Zn} or V_O. Indeed, its absence from our spectra could be explained by the large number of surface states expected in the ZnO nanocones. Such surface states are known to act as efficient electron traps that lead to strong charge carrier depletion and to very low electron density in the conduction band [30,44–46]. Indeed, previous studies of single ZnO NWs grown on crystalline Si using the same fabrication system and similar growth conditions as the ones used here have shown that the electrical resistance of the NW is very large and that it is reduced by several orders of magnitude when surface states are passivated with a MgO shell [35,37].

The ZnO EPR line around $g \sim 2$ observed in Fig. 5 is somehow difficult to analyze precisely due to its overlap with an electron resonance with similar g value coming from the PS substrate. We note that the large difference observed in the EPR spectra from ZnO/PS samples grown at different conditions mainly arises from changes in the PS substrates, which are sensitive to the different thermal treatments they have been subjected to during growth. This can be deduced from the EPR data for the bare substrates (Fig. 5(a) and (b)). Despite this, the simulations of the EPR spectra reveal that, in addition to the PS-related resonances at $g \sim 1.9997$, $g \sim 2.0035$ and $g \sim 2.0075$, a new line at $g \sim 2.006$ due to the ZnO nanocones is present. The g-factor values for PS around ~2.0035 and ~2.0075 have been attributed to the well known P_{b1} and P_{b0} centers, respectively, while, to our knowledge, the signal from PS around 1.9997 has not been previously reported. The $g \sim 2.006$ related to ZnO nanocones that dominates the EPR spectra for both ZnO/PS studied samples has been associated with a Zn divacancy interacting with one hole [43]. According to the results of the simulations, the relative contributions of the $g \sim 2.006$ resonance is 70% and 50% for the ZnO/PS samples grown with 8 sccm and 40 sccm of O_2, respectively. The signal associated with chemisorbed oxygen in ZnO ($g \sim 2.003$) [43] was not detected because it is masked by the strong PS resonance at $g \sim 2.0035$.

4. Conclusions

ZnO nanocones have been successfully deposited on PS by VT at different temperatures and O_2 flow rates without the need of typically used metallic nanocatalysts. Upon UV excitation, the ZnO/PS structures showed white light emission, potentially opening a venue for the development of white light illumination devices. The PL spectra could be deconvoluted into five components centered at about 1.84, 2.06, 2.30, 2.48 and 3.31 eV. The ZnO related emission components centered at 2.48 eV and 2.06 eV were attributed to charge carrier transitions involving oxygen vacancy states, while the emission at 2.3 eV was attributed to Zn vacancies. Luminescence centered at about 1.84 eV was attributed to the PS substrate. The relatively low excitonic emission in the UV and the observed rough ZnO nanocone surfaces suggest the presence of nonradiative recombination channels associated with surface trap states, which are known to cause strong carrier depletion in ZnO nanostructures. The absence from the EPR spectra of the $g = 1.96$ resonance, which is attributed to free electrons in the conduction band [42,43], supports the strong carrier depletion hypothesis, which in turn is consistent with a previous study of ZnO NWs [35]. Finally, an EPR line at $g \sim 2.006$, attributed to a Zn divacancy interacting with a hole in ZnO [43], is observed.

Acknowledgements

This work was supported by FONCyT (PICT 2010-0400), CIUNT 26/E419 and 26/E439, and FONARSEC TICs 2010/02.

References

[1] O. Bisi, S. Ossicini, L. Pavesi, Porous silicon: a quantum sponge structure for silicon based optoelectronics, Surf. Sci. Rep. 38 (2000) 1–126.
[2] A.B. Djurišić, A.M.C. Ng, X.Y. Chen, ZnO nanostructures for optoelectronics: material properties and device applications, Prog. Quantum Electron. 34 (2010) 191–259.

[3] M. Bengtsson, S. Ekström, G. Marko-Varga, T. Laurell, Improved performance in silicon enzyme microreactors obtained by homogeneous porous silicon carrier matrix, Talanta 56 (2002) 341–353.
[4] H.J. Zhang, H.M. Xiong, Biological applications of ZnO nanoparticles, Mol. Imaging 2 (2013) 177–192.
[5] E. Osorio, R. Urteaga, L.N. Acquaroli, G. García-Salgado, H. Juaréz, R.R. Koropecki, Optimization of porous silicon multilayer as antireflection coatings for solar cells, Sol. Energy Mater. Sol. Cells 95 (2011) 3069–3073.
[6] A. Al-Hajry, A. Umar, Y.B. Hahn, D.H. Kim, Growth, properties and dye-sensitized solar cells – applications of ZnO nanorods grown by low-temperature solution process, Superlattices Microstruct. 45 (2009) 529–534.
[7] S. Ozdemir, J.L. Gole, The potential of porous silicon gas sensors, Curr. Opin. Solid State Mater. Sci. 11 (2007) 92–100.
[8] X. Jiaqiang, C. Yuping, C. Daoyong, S. Jianian, Hydrothermal synthesis and gas sensing characters of ZnO nanorods, Sens. Actuators, B 113 (2006) 526–531.
[9] G.H. Du, F. Xu, Z.Y. Yuan, G. Van Tendeloo, Flowerlike ZnO nanocones and nanowires: preparation, structure, and luminescence, Appl. Phys. Lett. 88 (2006) 243101.
[10] Y. Gong, T. Andelman, G.F. Neumark, S. O'Brien, I.L. Kuskovsky, Origin of defect-related green emission from ZnO nanoparticles: effect of surface modification, Nanoscale Res. Lett. 2 (2007) 297–302.
[11] Z.L. Wang, Nanostructures of zinc oxide, Mater. Today 7 (2004) 26–33.
[12] G. Grinblat, M.G. Capeluto, M. Tirado, A.V. Bragas, D. Comedi, Hierarchical ZnO nanostructures: growth mechanisms and surface correlated photoluminescence, Appl. Phys. Lett. 100 (2012) 233116.
[13] C. Sandoval, O. Marin, S. Real, D. Comedi, M. Tirado, Electrophoretic deposition of ZnO nanostructures: Au nanoclusters on Si substrates induce self-assembled nanowire growth, Mater. Sci. Eng., B 187 (2014) 21–25.
[14] N.C. Vega, R. Wallar, J. Caram, G. Grinblat, M. Tirado, R.R. LaPierre, D. Comedi, ZnO nanowire co-growth on SiO2 and C by carbothermal reduction and vapor advection, Nanotechnology 23 (2012) 275602.
[15] M. Rajabi, R.S. Dariani, A. Iraji zad, Growth of ZnO nanostructures on porous silicon and oxidized porous silicon substrates, Braz. J. Phys. 41 (2011) 113–117.
[16] N. Rusli, M. Tanikawa, M. Mahmood, K. Yasui, A. Hashim, Growth of high-density zinc oxide nanorods on porous silicon by thermal evaporation, Materials 5 (2012) 2817–2832.
[17] H.I. Abdulgafour, F.K. Yam, Z. Hassan, K. Al-Heuseen, M.J. Jawad, ZnO nanocoral reef grown on porous silicon substrates without catalyst, J. Alloys Compd. 509 (2011) 5627–5630.
[18] C. Shaoqiang, Z. Jian, F. Xiao, W. Xiaohua, L. laiqiang, S. Yanling, X. Qingsong, W. Chang, Z. Jianzhong, Z. Ziqiang, Nanocrystalline ZnO thin films on porous silicon/silicon substrates obtained by sol–gel technique, Appl. Surf. Sci. 241 (2005) 384–391.
[19] R.G. Singh, S. Fouran, D. Kanjilal, V. Agarwal, R.M. Mehra, White light emission from chemically synthesized ZnO–porous silicon nanocomposite, J. Phys. D: Appl. Phys. 42 (2009) 062002.
[20] M. Kim, K. Yim, S. Kim, G. Nam, J.-Y. Leem, White light emission from nano-fibrous ZnO thin films/porous silicon nanocomposite, J. Sol-Gel. Sci. Technol. 59 (2011) 364–370.
[21] S. Hyun Lee, G. Earle Jellison, C.E. Duty, J. Xu, Light confinement-induced antireflection of ZnO nanocones, Appl. Phys. Lett. 99 (2011) 153113.
[22] J. Bae, J.-I. Hong, W.H. Han, Y.J. Choi, R.L. Snyder, Superior field emission properties of ZnO nanocones synthesized by pulsed laser deposition, Chem. Phys. Lett. 475 (2009) 260–263.
[23] Y.H. Yang, Y. Zhang, N.W. Wang, C.X. Wang, B.J. Li, G.W. Yang, ZnO nanocone: application in fabrication of the smallest whispering gallery optical resonator, Nanoscale 3 (2011) 592–597.
[24] T.K. Kundu, N. Karak, P. Barik, S. Saha, Optical properties of ZnO nanoparticles prepared by chemical method using Poly (VinylAlcohol) (PVA) as capping agent, Int. J. Comput. Eng. 1 (2011) 19–24.
[25] L. Shi, X. Li, Pure UV photoluminescence from ZnO thin film by thermal retardation and using an amorphous SiO2 buffer layer, J. Lumin. 131 (2011) 834–837.
[26] A.B. Djurišić, Y.H. Leung, K.H. Tam, L. Ding, W.K. Ge, H.Y. Chen, S. Gwo, Green, yellow, and orange defect emission from ZnO nanostructures: influence of excitation wavelength, Appl. Phys. Lett. 88 (2006) 103107.
[27] R.R. Koropecki, R.D. Arce, A.M. Gennaro, C. Spies, J.A. Schmidt, Kinetics of the photoinduced evolution of the nanostructured porous silicon photoluminescence, J. Non-Cryst. Solids 352 (2006) 1163–1166.
[28] T. Tamura, S. Adachi, Photo-oxidation effects of light-emitting porous Si, J. Appl. Phys. 105 (2009) 113518.
[29] W.M. Kwok, A.B. Djurišić, Y.H. Leung, W.K. Chan, D.L. Phillips, Time-resolved photoluminescence study of the stimulated emission in ZnO nanoneedles, Appl. Phys. Lett. 87 (2005) 093108.
[30] Z.M. Liao, H.-Z. Zhang, Y.B. Zhou, J. Xu, J.M. Zhang, D.P. Yu, Surface effects on photoluminescence of single ZnO nanowires, Phys. Lett. A 372 (2008) 4505–4509.
[31] Q. Zhu, C. Xie, H. Li, C. Yang, S. Zhang, D. Zeng, Selectively enhanced UV and NIR photoluminescence from a degenerate ZnO nanorod array film, J. Mater. Chem. C 2 (2014) 4566–4580.
[32] H.S. Kang, J.S. Kang, J.W. Kim, S.Y. Lee, Annealing effect on the property of ultraviolet and green emissions of ZnO thin films, J. Appl. Phys. 45 (2004) 1246–1250.
[33] Y.W. Heo, D.P. Norton, S.J. Pearton, Origin of green luminescence in ZnO thin film grown by molecular-beam epitaxy, J. Appl. Phys. 98 (2005) 073502.
[34] X. Yang, G. Du, X. Wang, J. Wang, B. Liu, Y. Zhang, D. Liu, D. Liu, H.C. Ong, S. Yang, Effect of post-thermal annealing on properties of ZnO thin film grown on c-Al2O3 by metal-organic chemical vapor deposition, J. Cryst. Growth 252 (2003) 275–278.
[35] G. Grinblat, F. Bern, J. Barzola-Quiquia, M. Tirado, D. Comedi, P. Esquinazi, Luminescence and electrical properties of single ZnO/MgO core/shell nanowires, Appl. Phys. Lett. 104 (2014) 103113.
[36] S. Panigrahi, A. Bera, D. Basak, Ordered dispersion of ZnO quantum dots in SiO2 matrix and its strong emission properties, J. Colloid Interface Sci. 353 (2011) 30–38.
[37] G. Grinblat, L.J. Borrero-González, L.A.O. Nunes, M. Tirado, D. Comedi, Enhanced optical properties and (Zn, Mg) interdiffusion in vapor transport grown ZnO/MgO core/shell nanowires, Nanotechnology 25 (2014) 035705.
[38] P. Jakes, E. Erdem, Finite size effects in ZnO nanoparticles: an electron paramagnetic resonance (EPR) analysis, Phys. Status Solidi RRL 5 (2011) 56–58.

[39] H. Kaftelen, K. Ocakoglu, R. Thomann, S. Tu, S. Weber, E. Erdem, EPR and photoluminescence spectroscopy studies on the defect structure of ZnO nanocrystals, Phys. Rev. B 86 (2012) 014113.
[40] C. Drouilly, J.M. Krafft, F. Averseng, S. Casale, D. Bazer-Bachi, C. Chizallet, V. Lecocq, H. Vezin, H. Lauron-Pernot, G. Costentin, ZnO oxygen vacancies formation and filling followed by in situ photoluminescence and in situ EPR, J. Phys. Chem. C 116 (2012) 21297–21307.
[41] K. Vanheusden, C.H. Seager, W.L. Warren, D.R. Tallant, J.A. Voigt, Correlation between photoluminescence and oxygen vacancies in ZnO phosphors, Appl. Phys. Lett. 68 (1996) 403–405.
[42] A.B. Djurišić, Y.H. Leung, W.C.H. Choy, K.W. Cheah, W.K. Chan, Visible photoluminescence in ZnO tetrapod and multipod structures, Appl. Phys. Lett. 84 (2004) 2635–2637.
[43] A.B. Djurišić, W.C.H. Choy, V.A.L. Roy, Y.H. Leung, C.Y. Kwong, K.W. Cheah, T.K. Gundu Rao, W.K. Chan, H. Fei Lui, C. Surya, Photoluminescence and electron paramagnetic resonance of ZnO tetrapod structures, Adv. Funct. Mater. 14 (2004) 856–864.
[44] Z.M. Liao, K.J. Liu, J.M. Zhang, J. Xu, D.P. Yu, Effect of surface states on electron transport in individual ZnO nanowires, Phys. Lett. A 367 (2007) 207–210.
[45] C.Y. Chen, J.R.D. Retamal, I.W. Wu, D.H. Lien, M.W. Chen, Y. Ding, Y.L. Chueh, C.I. Wu, J.H. He, Probing surface band bending of surface-engineered metal oxide nanowires, ACS Nano 6 (2012) 9366–9372.
[46] Y. Li, F. Della Valle, M. Simonnet, I. Yamada, J.J. Delaunay, Competitive surface effects of oxygen and water on UV photoresponse of ZnO nanowires, Appl. Phys. Lett. 94 (2009) 023110.